CrossMark

TECHNICAL ARTICLE

Development of Ultrafine-Grained Al–Mg–Si Alloy Through SPD Processing

Maruff Hussain[1] · P. Nageswara Rao[1] · R. Jayaganthan[1]

Abstract In the present investigation, ultrafine-grained Al alloy was produced from its bulk alloy by cryoforging followed by cryorolling. The bulk Al–Mg–Si alloy, with initial grain size 400 μm, was subjected to solid solution treatment (ST) followed by water quenching at room temperature. The ST treated alloy was subjected to aging at 100 °C for 4 and 8 h prior to cryoforging. The cryoforged alloy was subjected to cryorolling up to 2.4 true strain for producing long sheets. Finally, the deformed alloy was subjected to low temperature aging at 120 °C to improve the tensile properties of the alloys. Microstructure and mechanical properties were evaluated through Vickers hardness testing, tensile testing, and electron back scattered diffraction. The results have shown that combined cryoforging + cryorolling followed by aging led to remarkable improvement in strength (UTS-452 MPa) and ductility (8%). The average grain size of the alloy was found to be 240 nm, with increased fraction of high angle grain boundaries. Low temperature differential scanning calorimetry was used to study thermal behavior of bulk and severely deformed alloy.

Keywords Cryoforging · Cryorolling · Ultrafine-grained materials · Severe plastic deformation

✉ R. Jayaganthan
metarj@gmail.com

[1] Department of Metallurgical and Materials Engineering, Indian Institute of Technology Roorkee, Roorkee 247667, India

Introduction

The automobile industry is constantly demanding fuel efficient vehicles with pollution-free technologies to reduce the energy consumption as well as to ensure a clean environment. The reduction in vehicle weight by 10% could result in improvement of 8–10% in fuel economy [1]. The unique properties of aluminum alloys, such as high specific strength, good formability, high corrosion resistance, and recycling potential, make them ideal for replacing the heavier alloys currently used in vehicles in the automotive industries. Al–Mg–Si alloys are used for automotive body structures due to their good formability, high corrosion resistance, and better bake hardening response [1]. Among several Al alloys, more than 60% of them used in several structural and functional applications are based on 6xxx series [2]. Al–Mg–Si alloys are strengthened via dispersion of Mg_2Si nanosized precipitates through proper heat treatment. In order to meet the demand for materials with high strength to weight ratio, innovative processing techniques are being explored to enhance the strength of bulk alloys further. The common industrial practice is to reduce the grain size by adding grain refiners during the casting process [2, 3]. However, the minimum grain size achievable through the conventional routes is limited to a few microns. Recently, severe plastic deformation (SPD) techniques have been developed to reduce the grain size from micrometers to submicron or nanometer level by inducing severe strain into the material [4–8]. The size of samples that can be produced through SPD processes limits the use of ultrafine-grained materials (UFG) materials in practical applications. Multi-directional forging (MDF) is one potential technique used to produce UFG structures in the bulk materials. The samples size that can be produced through MDF is relatively large, which can be suitable for industrial applications [9]. It has been

successfully used to produce UFG structures in brittle material at elevated temperatures [10, 11].

In addition to large plastic strains induced by the SPD processes, deformation temperature plays critical role to promote grain refinement down to nanocrystalline range [12]. Medium and high stacking fault energy materials have been successfully processed through forging and rolling at cryogenic temperature (cryoforging and cryorolling) to achieve better grain refinement [12–15]. Cryorolling is one of the novel routes used to produce UFG structure in the bulk material with less induced plastic strain [8, 15–18]. On the other hand, hybriding of various SPD techniques could be exploited to produce UFG material in required shape with a desired grain size. In the SPD processes, the development of UFG structure occurs through generation and accumulation of dislocations, formation of cell structure, and its transformation to high-angle grain boundaries through consumption of continuously generated dislocations [19–21]. Deforming at cryogenic temperature retards the dislocation mobility and hence reduces the rate of dynamic recovery, results accumulation of high density of dislocations than the material deformed at room temperature [12, 15]. To date, there has been no systematic investigation on the development of UFG Al alloys through hybrid SPD processing techniques in the literature. Hence, the present work is focused on producing UFG microstructures in the bulk Al–Mg–Si alloys through combined cryoforging and cryorolling and realize the substantial improvement in tensile properties of the alloys as compared to its bulk Al alloys. Detailed microstructural characterizations of the SPD-processed alloys were performed to ensure the formation of thermally stable UFG microstructures in the Al–Mg–Si alloys. The improvement in tensile properties of the alloys has been elucidated through strengthening mechanisms arising from the grain size effect, dislocation hardening, solid-solution strengthening, and precipitation hardening.

Experimental Details

Commercially available Al–Mg–Si alloy was subjected to hybrid SPD for producing UFG microstructures in the alloy. Samples with dimension of $30.5 \times 27 \times 25$ mm^3 were machined from the as-received plate. They were subjected to solution treatment (ST) at 520 °C for 2 h. The quenched blocks are pre-aged at 100 °C for 4 and 8 h before subjecting them to MDF at cryogenic temperature. MDF was performed up to 4 cycles with a true strain of 2.4. These blocks were sectioned at center and further rolled at very low temperature by using liquid nitrogen (cryorolling) to achieve 1.5 mm thickness. A detailed procedure of MDF

at cryogenic temperature and cryorolling is reported in our earlier work [13]. Rolling alone is insufficient to induce high strain in the material and pure MDF also poses a problem during processing due to deviation of its original shape at high strains. Six sets of conditions with different combination of strain and heat treatments as shown in Table 1 were used to process the bulk Al–Mg–Si alloy. Figure 1 depicts the detailed processing methodologies adopted in the present work.

DSC Analysis

DSC analysis of deformed Al–Mg–Si alloys was performed by using low temperature differential scanning calorimetry under nitrogen atmosphere. Scans were performed with starting temperature of −5 °C, with heating rates of 10, 15, 20, 25 °C/min, up to a final temperature of 450 °C. For starting material in the ST condition, samples of 5 mm diameter weighing 30 mg were solid solution-treated and subsequently water quenched. They were immediately subjected to DSC measurements without any delay. The remaining conditions of samples were subjected to respective thermo-mechanical treatments followed by punching to 5 mm diameter sample with 30 mg weight. For all conditions, the surface finish of sample was maintained by grinding to 800 grit emery paper. Annealed pure Al was used as a reference sample. Base line correction was performed by subtracting the DSC heat flow curve of sample–reference from that of reference–reference.

Electron Back Scattered Diffraction (EBSD)

EBSD is used to investigate the microstructural evolution in different process conditions. Standard polishing procedures were adopted to polish the samples to a strain-free mirror-like surface. Etchant such as perchloric acid and methanol (20:80) with a voltage of 11 V for 90 s at −20 °C is used for polishing the sample required for EBSD analysis using FEI Quanta 200 FEG-SEM/EBSD. A step size of 0.1 μm was used for all EBSD scans.

Mechanical Characterization

Tensile testing was conducted with a strain rate of 9×10^{-4} s^{-1} on non-standard sub-size specimens. For MDF condition, the samples with gauge length, width and thickness of 10, 3 and 1.5 mm, respectively, were used. For all other conditions, the sample dimensions were; gauge length-17 mm, width-3 mm, and thickness-1.5 mm. Hardness measurements were performed on Vickers hardness testing machine with 5 kg load, dwell time of 15 s.

Table 1 Sample designation and their respective processing condition

| Designation	Processing condition
ST	Al–Mg–Si alloy solid solution treated at 520 °C for 2 h followed by cold water quenching
T6	ST material subjected to artificial aging at 177 °C for 8 h
ST1	ST material subjected to aging treatment at 100 °C for 4 h (pre aging)
ST2	ST material subjected to aging treatment at 100 °C for 8 h (pre aging)
MDF	ST material subjected to multi-directional forging at liquid nitrogen temperature up to 2.4 true strains.
MDF + PA	MDF after peak aging treatment
MDF1	ST1 material subjected to MDF followed by cryorolling up to 2.4 true strain
MDF1 + PA	MDF1 after peak aging treatment
MDF2	ST2 material subjected to MDF followed by cryorolling up to 2.4 true strain
MDF2 + PA	MDF2 after peak aging treatment
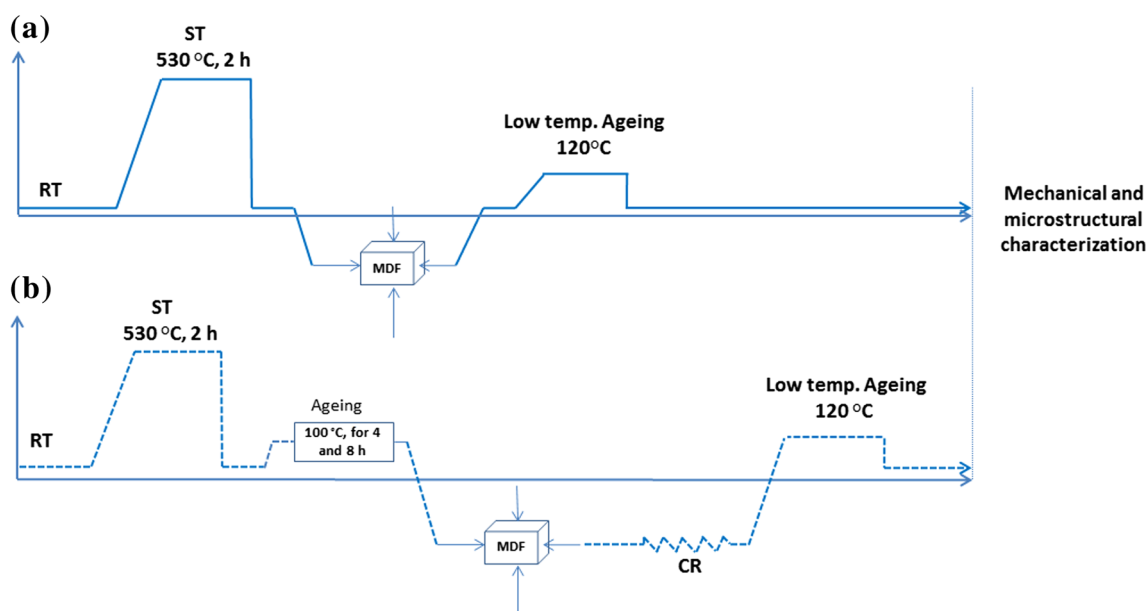
Fig. 1 Flow chart of various processes adopted in the present investigation; (**a**) MDF, (**b**) MDF1 and MDF2

Results and Discussion

Figure 2 shows the microstructure of the starting material after solution treatment. The average grain size is observed to be 400 μm. Figure 3 shows edge cracks developed in MDF1 and MDF2 samples due to severe strain. The thickness reduction per rolling pass is 0.4 mm. At initial passes of rolling, no edge cracks were observed, however, when the sheet becomes relatively thin and the ratio of sheet thickness to reduction per pass decreased the edge cracks become severe. This indicates the limitation in the rollability of the material further. Another reason could be reduced tensile ductility in the material due to pre-aging affect. Pre-aging is performed to form solute clusters, which helps in increasing the dislocation density in the material during rolling in the similar way what would be expected from a cryorolling process. It is also expected that these solute clusters suppresses the dynamic recovery through subgrain boundary pinning [22].

Hardness

Vickers hardness value of the ST material is 40 Hv (Table 2). After MDF, a 125% increase in hardness (90 Hv) was observed. The initial hardness of sample subjected to ST1 and ST2 conditions were found to be 56 and 62 Hv, respectively. The rise in hardness in ST1 with respect to aging time is more significant than that in ST2. The starting hardness values of MDF1 and MDF2 are 138 and 143 Hv, respectively, which are about 146 and 130% more than the
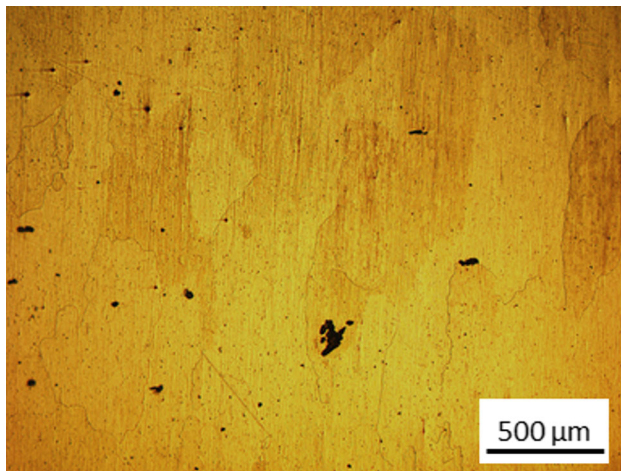
Fig. 2 Microstructure of starting material after solid solution treatment at 520 °C for 2 h (Etchant used: Poltons reagent)

Fig. 3 Photograph of UFG alloy sheets obtained through MDF1 and MDF2 routes

hardness value of starting material (ST1—56 Hv, ST2—62 Hv). The increase in hardness after MDF1 and MDF2 with respect to ST are 245 and 257%, respectively. The deformed sample was subjected to low temperature aging at 120 °C to improve its tensile properties due to precipitation hardening effect. As the strain induced in the material is very

high, aging temperature was selected as 120 °C for minimizing the recovery rate. Low temperature aging has led to a slight drop in hardness in MDF1 and MDF2 at initial stages, followed by nearly stable behavior with increasing aging time. On the other hand, in MDF and ST, an increase in hardness is observed from the beginning. Hardness plots are shown in Fig. 4(a).

Tensile Testing

Figure 4(b) shows the tensile plots of various conditions; test values are listed in Table 2. It is evident that the ST material possesses a large % elongation, low yield strength and remarkable work hardening behavior, which is typical of coarse-grained annealed material. After T6 treatment, the % elongation has dropped from 30 to 12% by increasing yield strength from 40 to 290 MPa. Whereas MDF has resulted increase in yield strength of the ST material from 40 to 265 MPa. The % of elongation at fracture is ∼10%. However, the uniform elongation is limited to ∼4% due to onset necking behavior which is typical of UFG metals processed by SPD [23]. The limited uniform elongation is attributed to low dislocation storage capability which results non-uniform elongation. It is also reported that the sample size has significant effect on post necking elongation (non-uniform elongation) [23]. Samples with smaller gauge lengths tend to show higher elongations [23].

The YS of MDF1 and MDF2 have increased significantly to 420 and 455 MPa. The total true strain accumulated in the material through MDF followed by rolling at liquid nitrogen temperature is 4.8. In addition to the low temperature deformation effect, pre-aging at 100 °C for 4 and 8 h led to formation of clusters, which would actively participate in pinning and accumulation of dislocations. Thus, the dislocation densities can be increased further in the pre-aged material as compared to un-aged material. MDF1 and MDF2 material exhibited elongations of 5 and 4.5%, respectively. The reduction in % elongations is as expected but the interesting observation is that the

Table 2 Mechanical properties of material subjected to various processing conditions

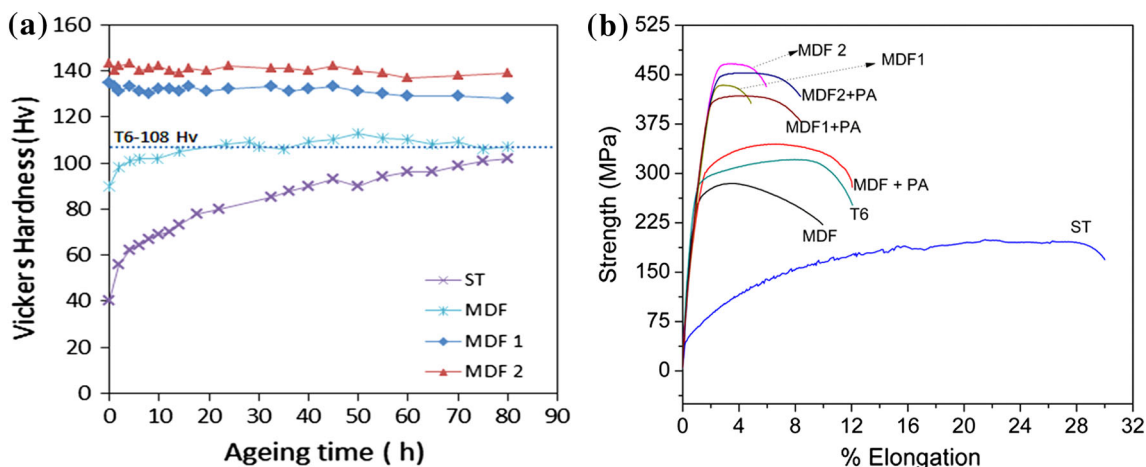| Processing condition	YS (MPa)	UTS (MPa)	% Elongation	Hardness (Hv)
ST	40	200	30	40
T6	290	325	12	108
MDF	265	286	10	90
MDF + PA	300	340	12	115
MDF1	420	426	5	138
MDF2	455	462	4.5	143
MDF1 + PA	400	415	8	133
MDF2 + PA	440	452	8	141

Fig. 4 Mechanical behavior of an alloy processed through various conditions; (**a**) Vickers hardness plots, (**b**) Plots of engineering stress versus engineering strain

elongation is of uniform in nature. The early stage of necking effect is comparable with MDF material.

Artificial aging has resulted opposite trends in the tensile behavior of bulk (ST) and UFG (MDF1 and MDF2) materials. With T6 treatment, % elongation has dropped but YS is increased compared to the ST material. On the other hand, UFG materials, upon aging treatment, show a drop in YS (from 420 to 400 MPa in MDF1 and 455 to 440 MPa in MDF2) but increase in % elongation (MDF1—3%, MDF2—3.5%). In MDF material, the trend is similar to the ST material. The effect of aging treatment on work hardening behavior is more significant than ductility in MDF material. The increase in uniform elongation after low temperature aging treatment in UFG materials (MDF, MDF1 and MDF2) is attributed to reduction in dislocation density and precipitation of high density of nanosized precipitates [24]. It can be concluded from the tensile plots that MDF1 and MDF2 processing conditions have produced remarkable improvement in strength (MDF1—415 MPa, MDF2—452 MPa) with reasonable ductility (8%).

DSC

Figure 5 shows DSC heat flow curves obtained with a heating rate of 15 °C/min for various processed conditions of bulk and UFG material. ST material (Fig. 5a) shows standard peaks that are observed commonly in Al–Mg–Si alloy. The widely accepted precipitation sequence in Al–Mg–Si alloys is Super saturated solid solution (SSSS) → Si–Mg–vacancy clusters → GP zones → $\beta'' \rightarrow \beta' \rightarrow \beta$ (Mg_2Si) [25–29]. The initial broad low temperature exothermic peak followed by two sharp exothermic peaks correspond to cluster formation, β'' phase formation (needle shaped, coherent with the matrix) and β' phase formation (rod shaped, semi

coherent with the matrix) respectively. The exothermic peak that appears near 450 °C could be due to β phase (incoherent, stable phase Mg_2Si), which is not significant for strengthening. After MDF, significant changes have occurred in the exothermic peak intensities and positions. The effect of cryogenic deformation on DSC heat flow behavior of Al 6061 alloy was reported in our earlier work [30]. The major difference observed in the present alloy, compared with common behavior of 6000 series alloys, is the behavior of β' phase. It is observed that deformation led to simultaneous formation of β' phase along with β'' phase, which has reduced the strengthening contribution from precipitation hardening mechanism to overall strengthening of the matrix [30–32]. In the present investigation, the appearance of distinguished peaks of β'' and β' signals showed a beneficial effect on strengthening. Comparing the position of the peaks in MDF material to ST material, the β'' peak has moved toward a lower temperature and β' has moved toward a higher temperature. This indicates that MDF has led to accelerated formation of β'' and delayed formation of β' phase. This phenomenon could cause the formation of stable β'' phase thereby reducing the earlier transformation to β' phase.

Figure 5(b) shows DSC heat flow curves of ST1 and MDF1 materials. Aging at 100 °C for 4 h caused reduced intensities of cluster peaks and slight variations in the intensities and positions of β'' and β' phase peak as compared to ST material. The behavior of heat flow curve of MDF1 material is slightly different from MDF material. There is shift in both β'' and β' phase peaks toward lower temperature, but with clear separation between them. The hump that appears in between 150 and 200 °C indicated the formation of GP zones [26, 32, 33]. Conditions favorable to form GP zones ought to be investigated in detail. After MDF1 samples were deliberately kept at room temperature to analyze the effect of small cluster peak that remained
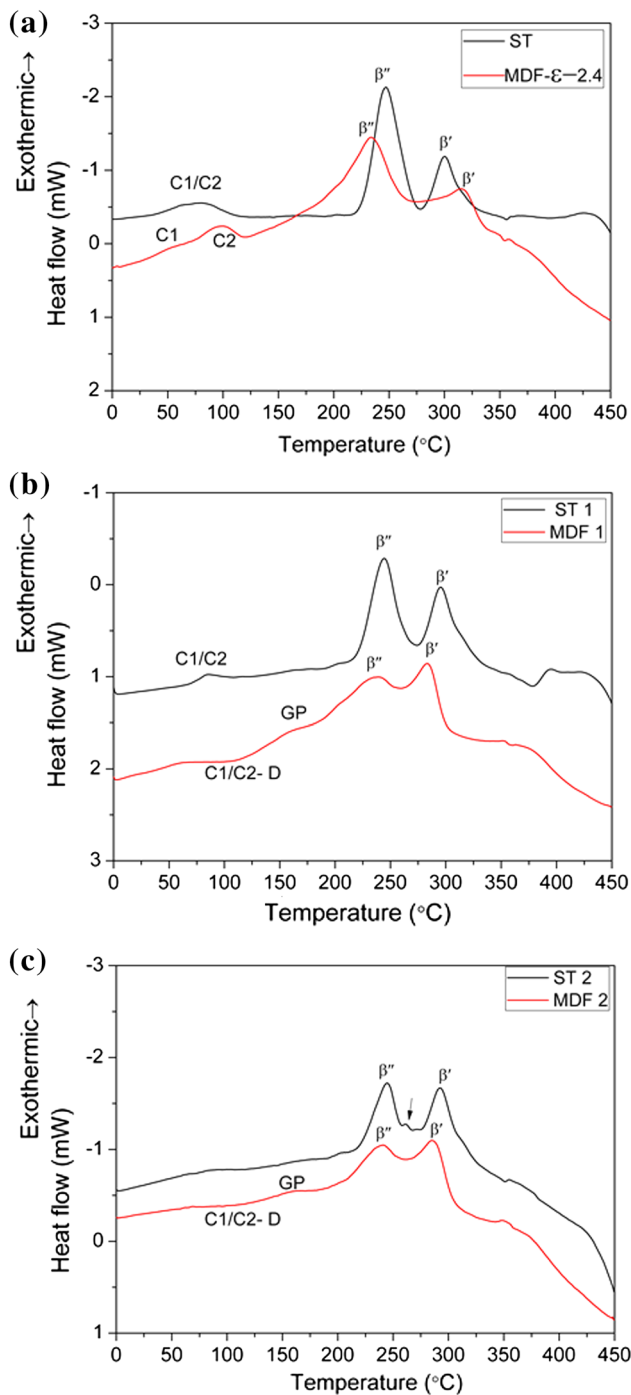
Table 3 Activation energies corresponding to β'' and β' phase evolution under various processing conditions

Condition	Activation energy (E) (kJ/mol)	
	β''	β'
ST	82	103.4
MDF	130	148
ST1	99	113
ST2	104	115
MDF1	109	153
MDF2	115	147

dissolved during DSC heating. The main purpose of performing aging at 100 °C is to develop stable clusters that which can grow further to β'' phase as well as to enhance the accumulation of dislocations during deformation. In 6000 series alloys it was observed that the clusters that form at room temperature during natural aging led to a delay in the formation of β'' particles and thereby lowers β'' volume fraction [34]. Ultimately this would influence the mechanical properties the alloy after final artificial aging treatment. The proposed practice to get rid of natural aging effect in 6000 series alloys is pre-aging at above room temperatures immediately after solid solution treatment [35–37]. Clusters that forms during pre-aging treatment are more stable and it will grow further to β'' phase during a bake hardening process [35]. This practice enhances the bake hardening response. In the present investigation, the appearance of a residue cluster peak, even after 4 h of aging at 100 °C, indicates the aging time and/or temperatures ought to be increased further for complete formation of clusters. The aging time has increased from 4 h to 8 h in the present study, which represented as ST2 condition.

Figure 5 (c) shows DSC heat flow curves of ST2 and MDF 2 material. The positions of the peaks are shifted further to lower temperatures as compared to former conditions. In addition to this, there is an additional small peak (indicated with arrow in Fig. 5c) in between the β'' and β' phase peaks. This has been checked with all heating rates and it has to be characterized in detail to determine the type of phase. At low temperatures, the cluster peaks are nearly suppressed. In MDF2 material, the behavior is similar to the MDF1 with very low intensity cluster dissolution peak.

Activation energies related to β'' and β' phase formations in various conditions are calculated by using Kissinger analysis from the peak temperatures obtained at various heating rates (10, 15, 20, 25 °C/min). The values are listed in Table 3. Pre-aging (ST1 and ST2) resulted in a slight increase in the activation energies with respect to ST material. At the same time, the activation energy values

Fig. 5 DSC heat flow curves of various processed conditions of an alloy with heating rate 15 °C/min; (**a**) ST and MDF, (**b**) ST1 and MDF1, (**c**) ST2 and MDF2. (*C1* cluster 1 formation, *C2* cluster 2 formation, *C1/C2-D* endothermic peak corresponding to clusters dissolution, *GP* peak corresponding to GP zones formation, β'', β' and β peaks corresponding to various phases of MgSi)

after aging at 100 °C. A small endothermic peak (Fig. 5(b), peak-C1/C2-D) that appeared between 50 and 150 °C indicates, the remnant solute after aging at 100 °C for 4 h, has formed clusters during natural aging. These clusters

associated with the formation of β'' and β' phase in deformed materials (MDF, MDF1 and MDF2) are also higher the ST material. Similar behavior has been reported in our earlier work [30]. Quainoo and Yannacopoulos have reported that the decrease in activation energy of β'' formation due to high strain energy induced in the material upon sever cold working [38]. The β'' phase improves the strength of the alloy depending up on the percentage of cold work. The slight differences in the strength of the alloy observed in the present work could be due to the difference in severity of deformation strain induced into the material and its subsequent influence on microstructural features such as large volume fraction of subgrain boundaries and high dislocation densities.

Fig. 6 EBSD microstructures of an alloy processed through various conditions; (**a**) MDF, (**b**) MDF + PA, (**c**) MDF1, (**d**) MDF1 + PA, (**e**) MDF2, (**f**) MDF2 + PA
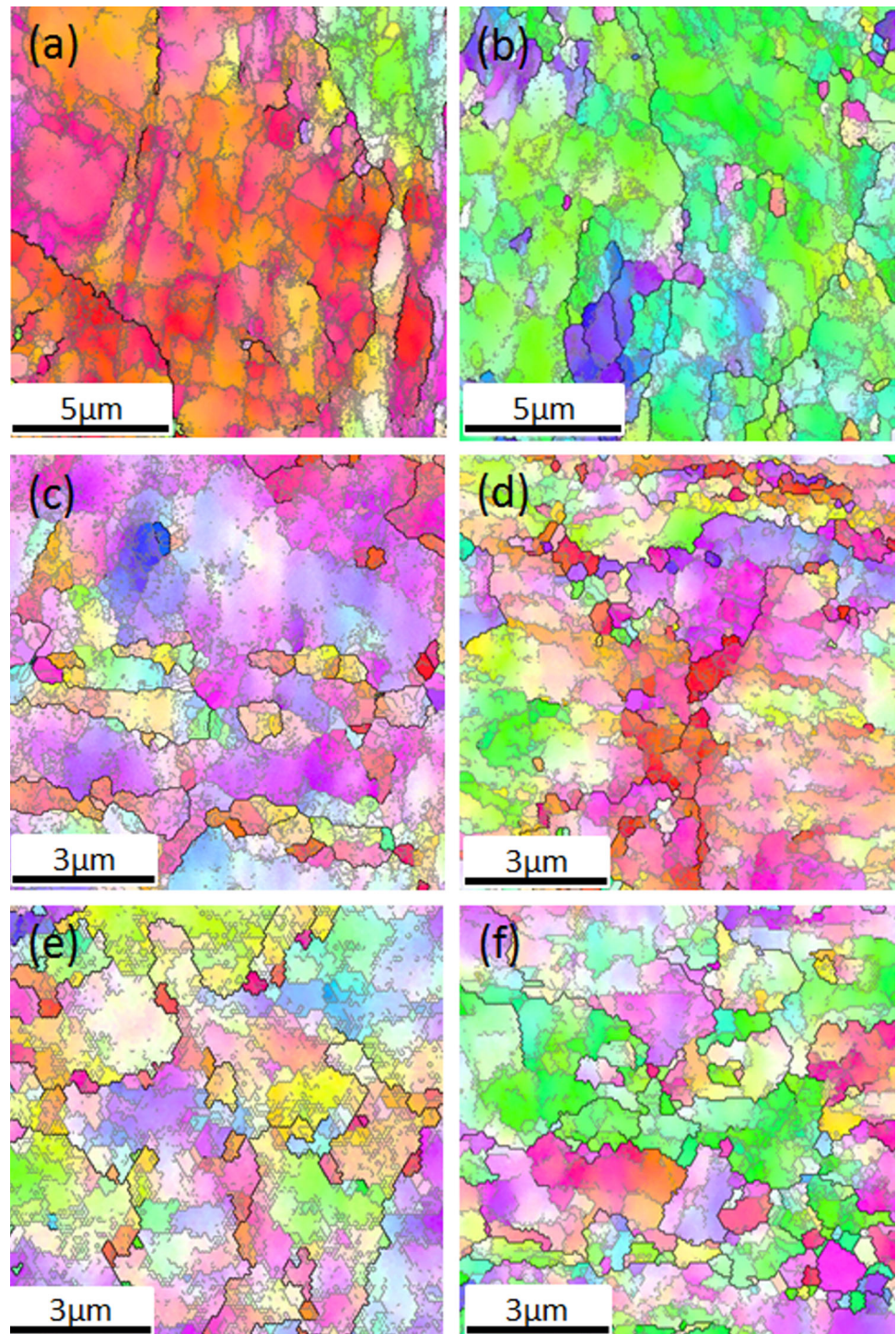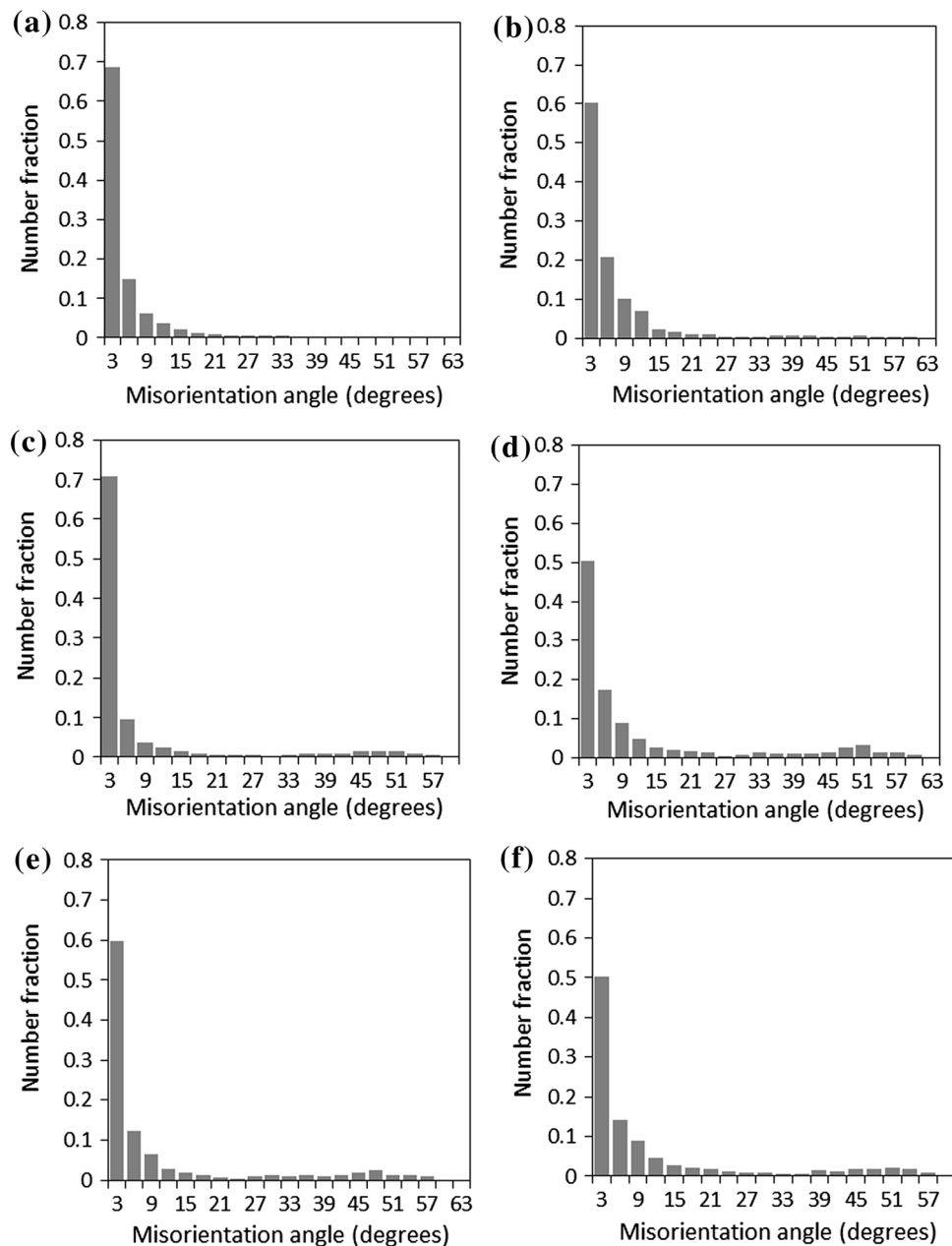
Fig. 7 Grain boundary misorientation plots an alloy processed through various conditions; (**a**) MDF, (**b**) MDF + PA, (**c**) MDF1, (**d**) MDF1 + PA, (**e**) MDF2, (**f**) MDF2 + PA

Microstructure

Microstructure analysis was carried out using EBSD for MDF, MDF1, MDF2 samples as well as in their respective peak aged conditions. Inverse pole figure maps and misorientation of grain boundaries data obtained through EBSD is shown in Figs. 6 and 7 respectively. As a common representation, black lines indicates high angle grain boundaries (Misorientation >15°) and gray lines indicates low angle grain boundaries (2° < Misorientation < 15°). The location of EBSD scan for MDF material is at the center of the central plane of the sample block. The inverse pole figure map shows that the MDF material possesses predominantly low angle grain boundaries. High angle grain boundaries can be observed at shear band structures due to strain localization. In MDF1 and MDF2 materials, the fraction of high angle grain boundaries is more as compared to MDF material. Another remarkable difference observed in MDF1 and MDF2 material is due to its decreased grain boundary spacing and increased dislocation density. The reduced recovery and enhanced dislocation pinning sites have led to accumulation of high density of dislocations in MDF1 and MDF2 materials. The prolonged aging at low temperature has enabled rearrangement of dislocations into dislocation cell boundaries in MDF material with no significant effect on high angle grain boundaries. The fraction of high angle grain boundaries has increased in MDF1 and MDF2 materials. The grain size

that observed in MDF1 and MDF2 materials are 270 and 240 nm, respectively. The grain size observed through EBSD is slightly higher than the actual size determined via through TEM due to the difference in spatial resolution.

Conclusions

In the present work, the Al–Mg–Si alloy was subjected to hybrid SPD processing (Cryoforging + Cryorolling) to produce UFG microstructures with improved mechanical properties. The microstructural characteristics and tensile properties of the deformed and aged alloys were investigated in details and the following conclusions are made

1. Employing pre-aging (100 °C for 4 and 8 h) has resulted significant improvement in strength and hardness in the MDF1 and MDF2 materials.
2. The material possesses a larger fraction of low angle grain boundaries even after deformation up to 4.8 true strain (in MDF1 and MDF2). This was attributed to suppression of dynamic recovery by rolling at very low temperature.
3. Low temperature aging of severely deformed material has resulted in slight drop in hardness (from 138 to 133 Hv in MDF1 and from 143 to 141 Hv in MDF2) at the beginning hours, later, the material possesses stable hardness. It indicates the balance between softening due to recovery and hardening due to precipitation. However, in lightly deformed material (MDF), the rise in hardness (from 90 to 115 Hv) with aging time is observed. It can be attributed to dominant precipitation hardening over softening by recovery.
4. Cold deformation has not suppressed the post β'' phase formation in ST, ST1, and ST2 materials but the peaks temperatures have varied.
5. Activation energy values of β'' and β' phases are significantly higher in pre-aged and deformed materials as compared to ST material.
6. The above conclusions indicate that the combination cryoforging and cryorolling can be used as a simple and cost-effective technique to produce high strength Al alloy sheets with UFG structure. Scheduling suitable heat treatments in precipitation hardenable alloys aids to achieve proper combination of properties.

References

1. W. Miller, L. Zhuang, J. Bottema, A. Wittebrood, P. De Smet, A. Haszler, A. Vieregge, Recent development in aluminium alloys for the automotive industry. Mater. Sci. Eng. A **280**(1), 37–49 (2000)

2. E. Wang, T. Gao, J. Nie, X. Liu, Grain refinement limit and mechanical properties of 6063 alloy inoculated by Al–Ti–C (B) master alloys. J. Alloys Compd. **594**, 7–11 (2014)

3. Y. Birol, Production of Al–Ti–B master alloys from Ti sponge and KBF4. J. Alloys Compd. **440**(1–2), 108–112 (2007)

4. R.Z. Valiev, T.G. Langdon, Principles of equal-channel angular pressing as a processing tool for grain refinement. Prog. Mater Sci. **51**(7), 881–981 (2006)

5. A. Zhilyaev, T. Langdon, Using high-pressure torsion for metal processing: fundamentals and applications. Prog. Mater Sci. **53**(6), 893–979 (2008)

6. H.W. Kim, S.B. Kang, N. Tsuji, Y. Minamino, Elongation increase in ultra-fine grained Al–Fe–Si alloy sheets. Acta Mater. **53**(6), 1737–1749 (2005)

7. S. Biswas, S. Suwas, Evolution of sub-micron grain size and weak texture in magnesium alloy Mg–3Al–0.4Mn by a modified multi-axial forging process. Scr. Mater. **66**(2), 89–92 (2012)

8. H. Yu, C. Lu, K. Tieu, X. Liu, Y. Sun, Q. Yu, C. Kong, Asymmetric cryorolling for fabrication of nanostructural aluminum sheets. Sci. Rep. **2**, 772 (2012)

9. K.B. Nie, K.K. Deng, X.J. Wang, F.J. Xu, K. Wu, M.Y. Zheng, Multidirectional forging of AZ91 magnesium alloy and its effects on microstructures and mechanical properties. Mater. Sci. Eng. A **624**, 157–168 (2015)

10. H. Miura, T. Maruoka, X. Yang, J.J. Jonas, Microstructure and mechanical properties of multi-directionally forged Mg–Al–Zn alloy. Scr. Mater. **66**(1), 49–51 (2012)

11. H. Miura, T. Maruoka, J.J. Jonas, Effect of ageing on microstructure and mechanical properties of a multi-directionally forged Mg–6Al–1Zn alloy. Mater. Sci. Eng. A **563**, 53–59 (2013)

12. Y. Wang, T. Jiao, E. Ma, Dynamic processes for nanostructure development in Cu after severe cryogenic rolling deformation. Mater. Trans. **44**(10), 1926–1934 (2003)

13. P.N. Rao, D. Singh, R. Jayaganthan, Mechanical properties and microstructural evolution of Al 6061 alloy processed by multi-directional forging at liquid nitrogen temperature. Mater. Des. **56**, 97–104 (2014)

14. Y. Nakao, H. Miura, T. Sakai, Microstructural evolution and recrystallization behavior in copper multi-directionally forged at 77 K. Adv. Mater. Res. **15–17**, 649–654 (2007)

15. Y. Wang, M. Chen, F. Zhou, E. Ma, High tensile ductility in a nanostructured metal. **419**, 912–915 (2002)

16. D. Singh, P. Nageswara Rao, R. Jayaganthan, Microstructural studies of Al 5083 alloy deformed through cryorolling. Adv. Mater. Res. **585**, 376–380 (2012)

17. E.V. Naidenkin, K.V. Ivanov, E.V. Golosov, Effect of cryorolling on the structure and the mechanical properties of ultrafine-grained nickel. Russ. Metall. **2014**(4), 303–307 (2014)

18. P. NageswaraRao, M. Gopi, R. Jayaganthan, Effect of cryorolling and ageing on microstructure, mechanical properties and corrosion behavior of Al–Cu–Mg–Si alloy. Banaras Met. **19**, 19–25 (2014)

19. Y. Estrin, A. Vinogradov, Extreme grain refinement by severe plastic deformation: a wealth of challenging science. Acta Mater. **61**(3), 782–817 (2013)

20. T. Sakai, H. Miura, X. Yang, Ultrafine grain formation in face centered cubic metals during severe plastic deformation. Mater. Sci. Eng. A **499**(1–2), 2–6 (2009)

21. R.Z. Valiev, R.K. Islamgaliev, I.V. Alexandrov, Bulk nanostructured materials from severe plastic deformation. Prog. Mater. Sci. **45**(2), 103–189 (2000)

22. M. Weiss, A.S. Taylor, P.D. Hodgson, N. Stanford, Strength and biaxial formability of cryo-rolled 2024 aluminium subject to concurrent recovery and precipitation. Acta Mater. **61**(14), 5278–5289 (2013)

23. Y.H. Zhao, Y.Z. Guo, Q. Wei, A.M. Dangelewicz, C. Xu, Y.T. Zhu, T.G. Langdon, Y.Z. Zhou, E.J. Lavernia, Influence of specimen dimensions on the tensile behavior of ultrafine-grained Cu. Scr. Mater. **59**(6), 627–630 (2008)

24. S. Cheng, Y.H. Zhao, Y.T. Zhu, E. Ma, Optimizing the strength and ductility of fine structured 2024 Al alloy by nano-precipitation. Acta Mater. **55**(17), 5822–5832 (2007)

25. A.K. Gupta, D.J. Lloyd, S.A. Court, Precipitation hardening processes in an Al–0.4%Mg–1.3%Si–0.25%Fe aluminum alloy. Mater. Sci. Eng. A **301**, 140–146 (2001)

26. G.A. Edwards, K. Stiller, G.L. Dunlop, M.J. Couper, The precipitation sequence in Al–Mg–Si alloys. Acta Mater. **46**(11), 3893–3904 (1998)

27. X. Wang, S. Esmaeili, D.J. Lloyd, The sequence of precipitation in the Al–Mg–Si–Cu alloy AA6111. Metall. Mater. Trans. A **37**, 2691–2699 (2006)

28. A. Gaber, M.A. Gaffar, M.S. Mostafa, E.F.A. Zeid, Precipitation kinetics of Al–1.12 Mg_2Si–0.35 Si and Al–1.07 Mg_2Si–0.33 Cu alloys. J. Alloys Compd. **429**(1–2), 167–175 (2007)

29. C. Marioara, S. Andersen, J. Jansen, H. Zandbergen, The influence of temperature and storage time at RT on nucleation of the β'' phase in a 6082 Al–Mg–Si alloy. Acta Mater. **51**(3), 789–796 (2003)

30. P.N. Rao, B. Viswanadh, R. Jayaganthan, Effect of cryorolling and warm rolling on precipitation evolution in Al 6061 alloy. Mater. Sci. Eng. A **606**, 1–10 (2014)

31. H.L. Lee, W.H. Lu, S.L.I. Chan, Effect of cold rolling on the aging kinetics of Al composite by differential scanning calorimetric technique. Scr. Metall. Mater. **25**(9), 2165–2170 (1991)

32. Y. Birol, The effect of sample preparation on the DSC analysis of 6061 alloy. J. Mater. Sci. **40**, 6357–6361 (2005)

33. C.S.T. Chang, J. Banhart, Low-temperature differential scanning calorimetry of an Al–Mg–Si alloy. Metall. Mater. Trans. A **42**(7), 1960–1964 (2011)

34. A. Cuniberti, A. Tolley, M.V.C. Riglos, R. Giovachini, Influence of natural aging on the precipitation hardening of an Al–Mg–Si alloy. Mater. Sci. Eng. A **527**(20), 5307–5311 (2010)

35. A. Serizawa, S. Hirosawa, T. Sato, Three-dimensional atom probe characterization of nanoclusters responsible for multistep aging behavior of an Al–Mg–Si alloy. Metall. Mater. Trans. A **39**(2), 243–251 (2008)

36. L. He, H. Zhang, J. Cui, Effects of pre-ageing treatment on subsequent artificial ageing characteristics of an Al–1.01 Mg–0.68Si–1.78Cu alloy. J. Mater. Sci. Technol. **26**(2), 141–145 (2010)

37. L. Cao, P.A. Rometsch, M.J. Couper, Effect of pre-ageing and natural ageing on the paint bake response of alloy AA6181A. Mater. Sci. Eng. A **571**, 77–82 (2013)

38. G.K. Quainoo, S. Yannacopoulos, The effect of cold work on the precipitation kinetics of AA6111 aluminum. J. Mater. Sci. **39**(21), 6495–6502 (2004)